

Available online at www.sciencedirect.com

International Journal of Solids and Structures 45 (2008) 2512–2533

INTERNATIONAL JOURNAL OF
SOLIDS AND
STRUCTURESwww.elsevier.com/locate/ijsolstr

Size effects of basic cell in static analysis of sandwich beams

G.M. Dai, W.H. Zhang*

Laboratory of Engineering Simulation and Aerospace Computing, The Key Laboratory of Contemporary Design & Integrated Manufacturing Technology, Ministry of Education, Northwestern Polytechnical University, P.O. Box 552, 710072 Xi'an Shaanxi, China

Received 10 March 2007; received in revised form 7 November 2007

Available online 23 December 2007

Abstract

In this paper, multilayered sandwich beam structures are considered. Within the scope of static analyses and stiffness design of such type of lightweight and functional structures, size effects of the basic cell are studied both theoretically and numerically in a systematic way for the first time. The direct FE discretization method, the homogenization method and the classical beam theory are examined systematically to reveal, on one hand, the existence of the size effect, and on the other hand, the ability of each method in capturing the size effect upon the static stress distribution and structural deflection. Particularly, limitations of the homogenization method are clarified although the latter is widely applied today in the equivalent modeling and topology design of cellular materials of sandwich structures. By means of the above methods, bending problems of multilayered beams and cellular core sandwiches are solved to illustrate variations of the deflection, stress as well as the computing accuracies in terms of the size of the basic cell. It is shown that the size effect is important when the basic cell has a considerable dimension relative to the structural size and that this effect decreases rapidly with the size reduction of the basic cell. Theoretically, the homogenized result corresponds to the limit solution when the size of the basic cell tends to be infinitely small.

© 2007 Elsevier Ltd. All rights reserved.

Keywords: Multilayered structure; Sandwich beam; Size effect; Homogenization method; Basic cell; Topology optimization

1. Introduction

To face the challenge of more and more complicated loading conditions, designs of lighter, safer and efficient structures with multi-functionality have been motivating researchers since a long time. Lightweight multilayered structures and sandwiches also called laminate panels belong to one such kind of advanced structures developed up to now. Geometrically, these structures can be considered as a result of periodic repetitions of a basic cell in one, two or three dimensions. A sandwich beam is an example of one dimensional repetitive structure along the longitudinal direction. In fact, beams and plates with repeating layers of specific materials can be treated as multilayered structures in a unified way. As shown in Fig. 1, a variety of sandwich structures with

* Corresponding author. Tel.: +86 (0)29 88495774; fax: +86 (0)29 88495774.

E-mail address: Zhangwh@nwpu.edu.cn (W.H. Zhang).

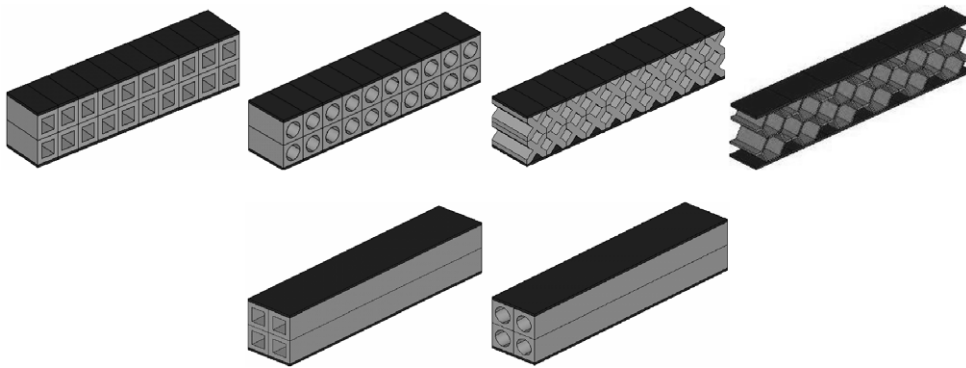


Fig. 1. Sandwich structures of different basic cell configurations.

different cell configurations and arrangements are illustrated (see Romanoff and Varsta, 2006; Hayes et al., 2004).

Actually, extensive applications of multilayered structures are found in aerospace industries as optical, biological, microelectronic, heat-resisting and thermo-mechanical components due to their high stiffness, superior strength/toughness, heat insulation, lightweight properties, etc. To explore these functionalities and advantages, it is essential to have a deep understanding about the geometrical and material factors that influence the mechanical behaviors of the structure. The state of the art of existing works may be briefly summarized below. Noor et al. (1996) gave a comprehensive review of different computational models on sandwich panels and shells. Applications were involved in problems of heat transfer, thermal and stresses, free vibration and damping, transient dynamic responses, design optimization, etc. Khdeir and Reddy (1997) investigated the static deflection of laminated composite beams for which the classical, first-order, second-order and third-order beam theories have been used in the analysis. It is shown that the Euler–Bernoulli classical beam theory agrees well with high-order theories for thin beams with large length-to-height ratio. But large differences exist between the classical beam theory and high-order theories for short or thick layered beams when the length-to-height ratio is large with important effect of shear deformation. The disagreement between high-order theories is much less than the disagreement between any of them and the Euler–Bernoulli theory. Burton and Noor (1997) investigated numerically the accuracy of three continuum models of the honeycomb core, i.e., lower bound energy approach, upper bound energy approach and design-data test based approach when the honeycomb core is substituted with an effective continuum in the dynamic analysis of sandwich panel. The free vibration responses predicted by the detailed FE model were used as the standard of comparison. Due to the expensive computing cost of detailed finite element modeling, the cellular core was generally modeled by an equivalent continuum of effective properties. Therefore, to ensure the computing accuracy, it is important to make evidence necessary conditions to be satisfied for one such homogenization equivalence. In fact, the homogenization method reported by Bensoussan et al. (1978), Sanchez-Palencia (1980), and Bakhvalov and Panasenko (1989) is a specific two-scale approach used to predict the equivalent properties of composite materials. It is theoretically formulated as an asymptotic expansion of small parameter under the assumption of periodic distribution of the basic cell. Hassani and Hinton (1998) gave a review of the homogenization theory and its applications in topology optimization of structures and cellular materials.

Meraghni et al. (1999) only evaluated the effective out-of-plane elastic constants of hexagonal honeycomb core by means of direct FE analysis, analytical laminate theory and experimental tests. The in-plane bending stiffness is however not taken into account. As the configuration remains unchanged along the thickness direction of the honeycomb core and can be considered to have an infinite periodicity in this direction, the effective out-of-plane elastic constants evaluated by the analytical laminate theory are found to be free from the honeycomb thickness and agree exactly with those obtained by the homogenization method. Recently, Hsueh et al. (2006) studied the biaxial strength of thin multilayered disks. An analytical model of general closed-form solutions is developed for the elastic stress distributions subjected to biaxial flexure tests. The model is verified by the FE analysis of trilayered disks subjected to ring-on-ring tests.

Ashby (1999), Ashby and Bréchet (2003), and Pasini (2006) introduced the concept of shape factor or shape transformer as a dimensionless parameter to measure the structural efficiency in terms of geometric quantities of a beam cross-section regardless of size. With the combination of the material indices, this approach provides a practical way to develop selection charts for integrated shape and material optimum design of cross-sections. Inspired from the composition of natural or biological materials that have a complex hierarchical cell arrangement of different sizes, Burgueno et al. (2005) studied the designs of hierarchical cellular sandwich beams and plates with high structural efficiency. Based on experimental tests of cellular plates with different densities of porosity and different hole arrangements over the cross-section, the measured results of effective elastic constant related to the bending stiffness showed a good agreement with the shape factors and material indices. Kolpakov (2001) dealt with the discrete and continuous distribution designs of material properties in each layer of laminated plates. The design model is formulated as a convex combination problem (CCP) to match the stiffness given a priori. Alternatively, Wang and McDowell (2003) and Hayes et al. (2004) studied extruded metal honeycombs, i.e., the so-called linear cellular alloys (LCA). The first work was focused on the maximization design of elastic torsion and bending rigidities of the circular sandwich bar structure in terms of the triangular subcell geometry of the sandwich core while the second work was to understand the heat transfer and mechanical behaviors of the LCA. Besides, it is also important to refer to certain works on FGM materials (e.g., Abrate, 2006) that belong to also a sort of multilayered structures with the same concerns.

Behind the calculations and measurements of mechanical properties of sandwich panels, the effect of the specimen size relative to the cell size, i.e., the size effect was addressed by Onck et al. (2001) for the in-plane elastic constants of hexagonal honeycombs. Based on the finite element modeling and experimental tests, the size effect was found to be important when the macroscopic dimensions of the specimen become of the order of the microstructural length scale of the material. This effect arising from both a change in the constraint of the cell walls at the boundary of a specimen and stress-free cut cell edges at the surface of a specimen results in an increase of the in-plane elastic constants with an increasing ratio of the specimen size to the cell size, up to a plateau level in the limit case. Tantikom et al. (2005) obtained the same conclusion for the size effect from the compression test of tubular core.

Despite the popularity of homogenization method applied in topology design optimization (Neves et al., 2002; Fujii et al., 2001; Bendsøe and Sigmund, 2003), few studies have been made about the size effect upon topology design solution so far. Bendsøe and Triantafyllidis (1990) studied the elastic buckling design in terms of the cell size. Recently, Zhang and Sun (2006) studied the size effect upon the optimal configuration of core material microstructure in the rigidity optimization of 2D sandwich problems. The super-element technique was used and numerical results show that the optimum configuration of the cellular core varies in terms of cell size and is therefore scale related. Such a scale effect cannot however be revealed by the traditional homogenization method.

As the cell size is an intrinsic factor of the sandwich structure, what is the underlying relationship between the mechanical behaviors and the cell size, especially, what about the asymptotic values of structural stiffness, structural responses and their relationship with the homogenization solutions when the cell size tends to be infinitely small constitute essential problems that have not been clarified profoundly until now. Besides, in the emerging researches on ultra-light weight structures under complex loading conditions for aerospace applications, the advanced design of porous core sandwich structures requires greatly the development of reliable optimization procedures for the integrated design of materials and structures. In such a procedure, the homogenization method used to predict effective properties, e.g., the elastic tensor, thermal expansion coefficients, heat conduction coefficients, etc. is unable to reflect the size effect of the basic cell. Only the porosity and the microstructural configuration are involved in the computation. This implies that the method is valid only asymptotically when the cell size of the material microstructure is very small in comparison with the macro-size of the structure. Otherwise, the homogenization can lead to incorrect values. In reality, this limit size is never reached because the actual size of the basic cell is never infinitely small and the macrostructure size is nor infinitely large. Meanwhile, the cell size is also an important parameter to be determined before setting up the manufacturing process. Therefore, it is of great interest to understand deeply the size effect from the design point of view. This is the motivation of the current work. To this end, the direct FE method, the homogenization method and classical laminate theory will be employed systematically for the common test

problems. With obtained computing results, each method is highlighted in a comparative way to show the difference between each of them.

Here, a great number of examples are presented to show the size effects of the basic cell, e.g., the influences upon the structural static deflections and stress distributions. With the classical beam theory, it is shown that the size effect upon the static performance of sandwich structures can be analytically figured out and the computing accuracies of FE analysis and homogenization method can be easily made in evidence. This will offer an important basis for the optimal design and multi-functionality service of sandwich structures.

2. Static analysis of sandwich beam structures

Here, sandwich beam structures may refer to multilayered structures with symmetrical cross-sections, such as web-core sandwich and cellular core beam structures. Suppose the considered sandwich structure is generated by a periodic distribution of unit cells, each of which has a specific microstructure composed of multiple material phases. Note that the void can be regarded as a material phase. From the design point of view, studies are focused on the size effect of the unit cell upon static responses under loading conditions. Here, the variation of the cell size will result in only the variation of cell numbers while the microstructure and the volume fraction of each phase material involved in the basic cell remain unchanged. Naturally, a decrease of the cell size corresponds to an increase of the cell number. To figure out the problem, consider firstly the bending of a multilayered beam as an illustrated below.

2.1. Analytical method for size effect-related static analysis

Without loss of generality, consider a simple example of a multilayered beam of rectangular cross-section as shown in Fig. 2. The cross-section consists of periodic unit cells of bi-phase materials and each unit cell contains three layers of materials. Suppose the volume fraction of each material phase, i.e., the proportion ratio, is fixed. With the increase of the cell number n , a multilayer stack is generated in the transversal direction so that the thickness of each phase material will reduce correspondingly. Thus, n can be considered as a scale factor

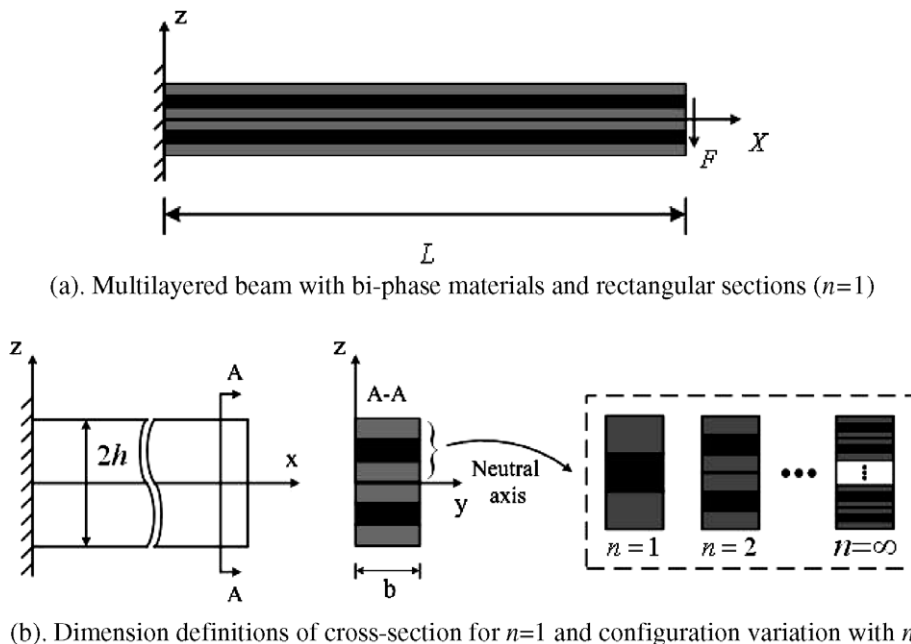


Fig. 2. Illustration of a multilayered beam.

characterizing the refinement of layer thickness that, in turn, changes the lamination effect. The scale effect is to study how the structural responses will change in terms of n with the fixed material volume fraction. Bending and stretch cases are considered now.

2.1.1. Bending

Under the assumption of Euler–Bernoulli beam, the deflection of a beam caused by the bending moment M is dominated by the following differential equation

$$D \frac{d^2 w(x)}{dx^2} = M(x) \quad (1)$$

Hence, related stresses and strains are expressed as

$$\sigma(x) = E(x)\varepsilon(x) = E(x) \frac{M(x)z(x)}{D}, \quad \tau = E(x) \frac{Q(x)S}{Db} \quad (2)$$

$$\varepsilon(x) = \frac{M(x)z(x)}{D} \quad (3)$$

Q is the shear force. b is the beam width. S is the first moment of the area. D stands for the flexural rigidity depending upon the location variable x , Young's modulus E of each constitutive phase material and the cross-sectional shape characterizing how materials are distributed.

Consider $n = 1$ for the cross-section specified in Fig. 2(b), the flexural rigidity is then

$$D^{(1)} = \sum E_i I_i = \frac{2}{3} E_1 b \left[\left(\frac{2h}{3} \right)^3 - \left(\frac{h}{3} \right)^3 \right] + \frac{2}{3} E_2 b \left\{ \left[h^3 - \left(\frac{2h}{3} \right)^3 \right] + \left(\frac{h}{3} \right)^3 \right\} \quad (4)$$

where b denotes the beam width. E_i is the Young's modulus of material phase i .

Generally, the following relation can be deduced for a n -number of unit cells

$$D^{(n)} = \sum E_i I_i = 2E_1 \cdot \frac{1}{3} b \sum_{m=1}^n \left[\left(\frac{(3m-1)h}{3n} \right)^3 - \left(\frac{(3m-2)h}{3n} \right)^3 \right] + 2E_2 \cdot \frac{1}{3} b \sum_{m=1}^n \left\{ \left[\left(\frac{mh}{n} \right)^3 - \left(\frac{(3m-1)h}{3n} \right)^3 \right] + \left[\left(\frac{(3m-2)h}{3n} \right)^3 - \left(\frac{(m-1)h}{n} \right)^3 \right] \right\} \quad (5)$$

and the compact form is

$$D^{(n)} = \frac{2}{3} b E_1 \left(\frac{1}{3} - \frac{2}{27n^2} \right) h^3 + \frac{2}{3} b E_2 \left(\frac{2}{3} + \frac{2}{27n^2} \right) h^3 \quad (6)$$

For $h = 3$, the concise expression reads

$$D^{(n)} = 6bE_1 - \frac{4bE_1}{3n^2} + \frac{4bE_2}{3n^2} + 12bE_2 \quad (7)$$

This is a reciprocal function of n . When $n \rightarrow \infty$, the flexural rigidity of the beam becomes

$$D^{(\text{inf})} = \sum EI = 6bE_1 + 12bE_2 \quad (8)$$

Correspondingly, the beam deflection attains its minimum value at $x = L$.

$$w_{\text{max}}^{\text{inf}} = \frac{FL^3}{3D^{\text{inf}}} = \frac{FL^3}{18b(E_1 + 2E_2)} \quad (9)$$

Scale effects are illustrated in Fig. 3. For small values of n , influences are important and a sharp variation exists. When $n > 5$, the scale effect is negligible. The limit value of flexural rigidity equals 4.62×10^{11} for $n \rightarrow \infty$.

As to the bending stress, it is obtained from Eq. (2)

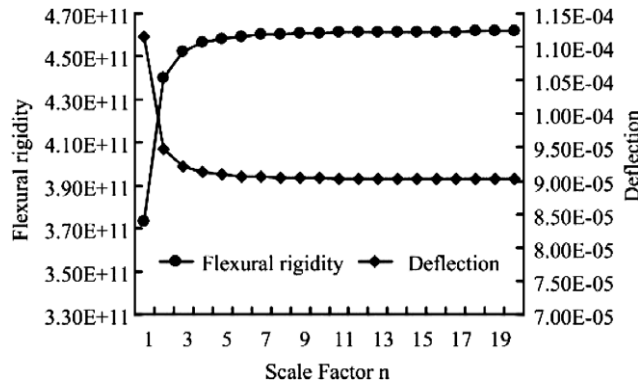


Fig. 3. Flexural rigidity and deflection versus n ($E_1 = 70 \times 10^9$, $E_2 = 3.5 \times 10^9$, $F = 1000$).

$$\sigma = \frac{Mz}{D^{(n)}} E_i = \frac{F(L-x)z}{D^{(n)}} E_i = F(L-x)z E_i \left(6bE_1 - \frac{4bE_1}{3n^2} + \frac{4bE_2}{3n^2} + 12bE_2 \right)^{-1} \tag{10}$$

At $x = L/2$, the distribution along the thickness direction is shown in Fig. 4. Clearly, the discontinuity is due to the material discontinuity.

Similarly, the shear stress evaluated from Eq. (2) is shown in Fig. 5 for different values of n .

2.1.2. Stretch

Under the assumption of uniform stress distribution over the cross-section, the stretch rigidity along longitudinal direction can be easily obtained as

$$A^{(n)} = \sum \int_{h_{k-1}}^{h_k} E b dz = 2E_1 \cdot b \sum_{m=1}^n \left[\left(\frac{(3m-1)h}{3n} \right) - \left(\frac{(3m-2)h}{3n} \right) \right] + 2E_2 \cdot b \sum_{m=1}^n \left\{ \left[\left(\frac{mh}{n} \right) - \left(\frac{(3m-1)h}{3n} \right) \right] + \left[\left(\frac{(3m-2)h}{3n} \right) - \left(\frac{(m-1)h}{n} \right) \right] \right\} \tag{11}$$

So we have

$$A^{(n)} = \frac{2bh}{3} (E_1 + 2E_2) \tag{12}$$

Obviously, the stretch rigidity is independent of the scale factor n .

2.2. Homogenization method

For a unit cell of anisotropic materials, the effective stress tensor $\bar{\sigma}_{ij}$ and strain tensor $\bar{\epsilon}_{kl}$ are interrelated by

$$\bar{\sigma}_{ij} = C_{ijkl}^H \bar{\epsilon}_{kl} \tag{13}$$

where C_{ijkl}^H is the effective, also termed homogenized, elastic tensor to be evaluated.

The homogenization method is based on a two-scale asymptotic expansion of structural responses with periodic material unit cells. Only a brief description is given here and detailed demonstrations can refer to Bensoussan et al. (1978) and Sanchez-Palencia (1980). To describe the fast variation of material properties in the macro-scale (X), a micro-scale coordinate system (Y) is introduced to detail the material microstructure. The length measured in Y can be regarded as an amplification of that measured in X so that $y = \frac{x}{\epsilon}$ with parameter

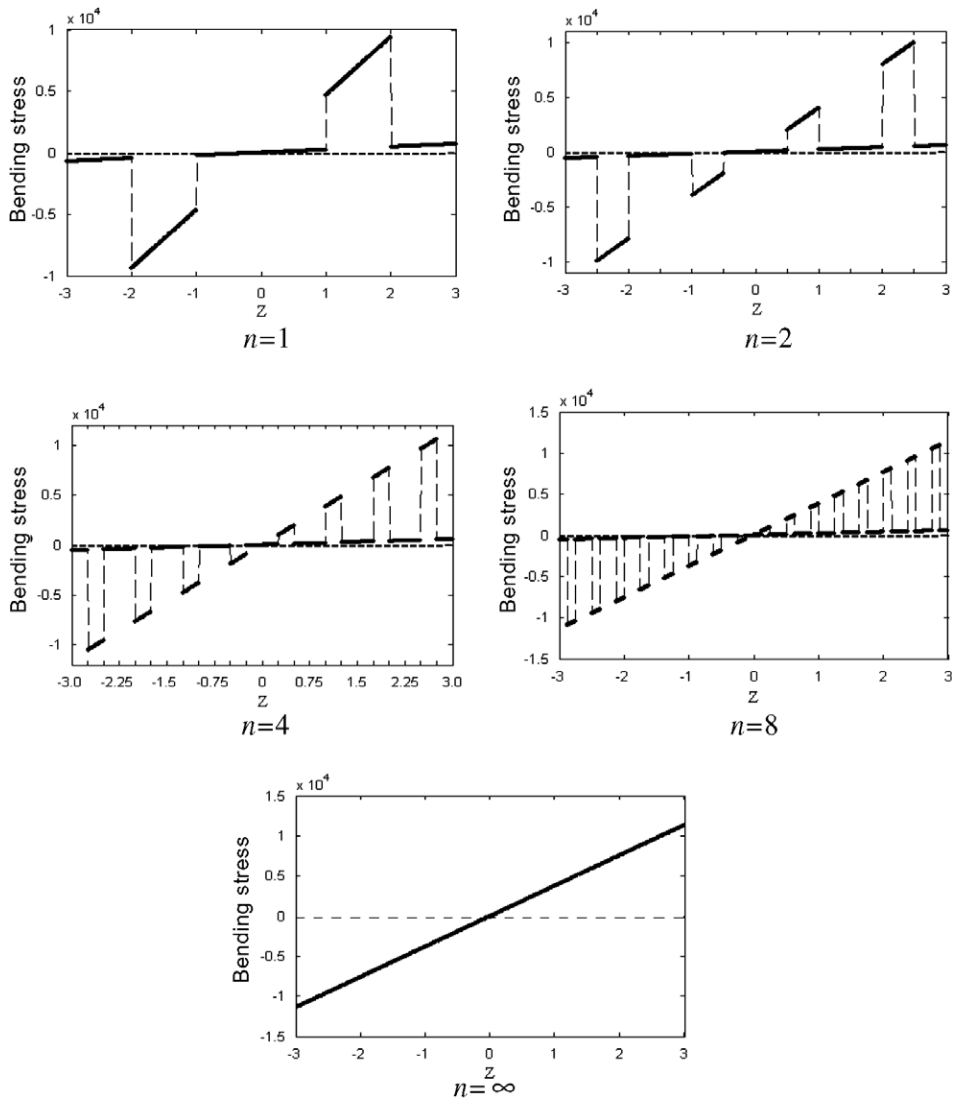


Fig. 4. Bending stress distribution at $x = L/2$.

$\varepsilon \ll 1$. Therefore, the displacement of an arbitrary material point in an elastic body can be approximated by an asymptotic expansion with

$$u^\varepsilon(x) = u^0(x, y) + \varepsilon u^1(x, y) + \varepsilon^2 u^2(x, y) + \dots \tag{14}$$

Briefly, the substitution into the equilibrium equation system allows for obtaining

$$C_{ijkl}^H = \frac{1}{|Y|} \int_Y \left(C_{ijkl} - C_{ijpq} \frac{\partial \chi_p^{kl}}{\partial y_q} \right) dY \tag{15}$$

Here, $|Y|$ denotes the volume of the unit cell. χ^{kl} is a Y -periodic admissible displacement field associated with load case kl . χ^{kl} is obtained from the following integral equation over the unit cell with periodic boundary conditions.

$$\int_Y C_{ijpq} \frac{\partial \chi_p^{kl}}{\partial y_q} \frac{\partial v_i}{\partial y_j} dY = \int_Y C_{ijkl} \frac{\partial v_i}{\partial y_j} dY \quad \forall v \in Y \tag{16}$$

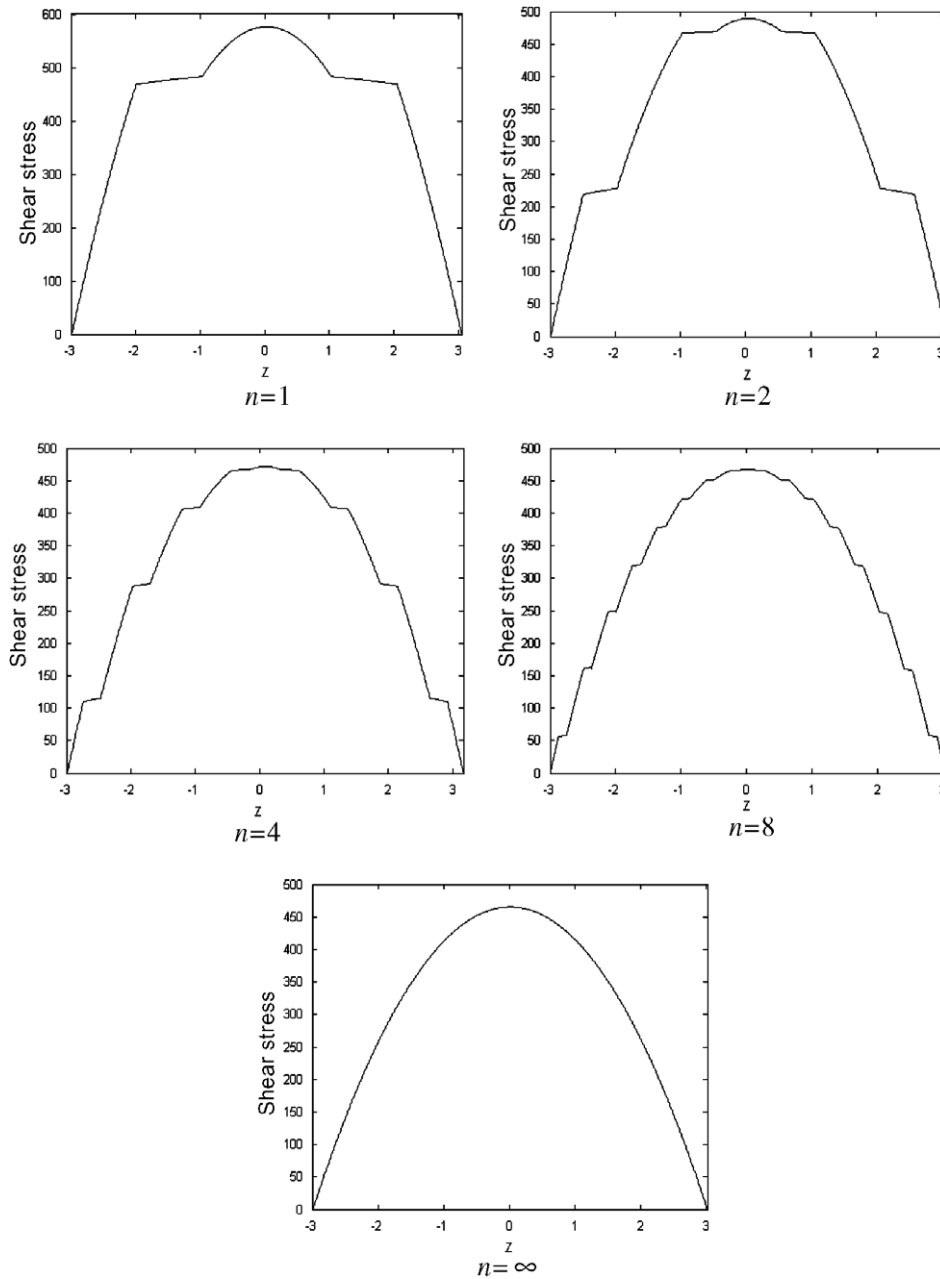


Fig. 5. Shear stress distribution at $x = L/2$.

with v to be a kinematically admissible arbitrary displacement field.

Numerically, χ^{kl} is computed over the unit cell by the FE analysis procedure in which corresponding loads are obtained as the jump of elastic material properties along the interfaces between distinct constitutive phases. For example, 3 load cases exist for 2D plane stress problems with $kl = 11, 22, 12$ and 6 load cases exist for 3D problems with $kl = 11, 22, 33, 12, 13, 23$. Hence, Eq. (15) can be numerically evaluated with the following computing scheme

$$C_{ijkl}^H = \frac{1}{|Y|} \int_Y \left(C_{ijkl} - C_{ijpq} \frac{\partial \chi_p^{kl}}{\partial y_q} \right) dY = \langle C_{ijkl} \rangle - \langle \sigma_{ij}^{kl} \rangle \quad (17)$$

where $\langle C_{ijkl} \rangle$ denotes the averaged elastic tensor depending upon only the material volume fractions of constituents as in the classical mixture rule whereas $\langle \sigma_{ij}^{kl} \rangle$ denotes the averaged stress tensor over the unit cell in load case kl . Obviously, $\langle \sigma_{ij}^{kl} \rangle$ is a correction term that reflects the influence of the material microstructure of the unit cell.

As the microstructure of the unit cell illustrated in Fig. 2 is a rank-1 material with a periodic alternation only in the thickness direction, the effective elastic tensor can be obtained analytically by homogenization method. Based on the work of Hassani and Hinton (1998), terms of the effective elastic tensor for a unit cell of bi-layer materials shown in Fig. 6(a) with thickness γ and $1 - \gamma$, respectively, are given by.

If both phases are isotropic materials with the same Poisson’s ratio and different Young’s moduli E_I and E_{II} , it then follows that

$$C_{1111}^i = C_{2222}^i = \frac{E_i}{1 - \nu^2}; \quad C_{2211}^i = \frac{\nu}{1 - \nu^2} E_i; \quad C_{1212}^i = \frac{E_i}{2(1 + \nu)} \quad (i = I, II) \tag{18}$$

The effective elastic terms given in Table 1 can be simplified as Table 2.

In fact, the above relations given by Hassani and Hinton (1998) can be extended to the unit cell of three layers as that shown in Fig. 6(b). The Arithmetic average operator \bar{A} and the Harmonic average \underline{A} can be firstly defined by

$$\bar{A}(r_1, r_2, r_3, \xi_1, \xi_2, \xi_3) = \xi_1 r_1 + \xi_2 r_2 + \xi_3 r_3, \quad \underline{A}(r_1, r_2, r_3, \xi_1, \xi_2, \xi_3) = \frac{r_1 r_2 r_3}{\xi_1 r_2 r_3 + \xi_2 r_1 r_3 + \xi_3 r_2 r_1} \tag{19}$$

where $\xi_1, \xi_2, \xi_3 \in [0, 1]$ and r_1, r_2, r_3 are three real numbers.

Then, it can be demonstrated that the homogenized terms of elastic tensor related to Fig. 6(b) can be expressed as Table 3.

Note that

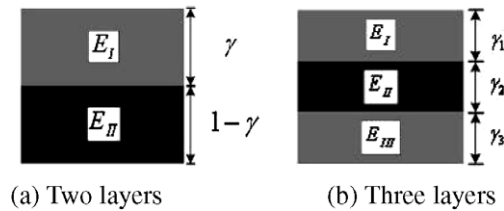


Fig. 6. Rank-1 material.

Table 1
Homogenized elastic tensor for rank-1 material

$$C_{1111}^H = \gamma C_{2222}^I + (1 - \gamma) C_{2222}^{II} - [\gamma (C_{2211}^I)^2 (C_{1111}^I)^{-1} + (1 - \gamma) (C_{2211}^{II})^2 (C_{1111}^{II})^{-1}] + [\gamma C_{2211}^I (C_{1111}^I)^{-1} + (1 - \gamma) C_{2211}^{II} (C_{1111}^{II})^{-1}]^2 \cdot \frac{C_{1111}^I C_{1111}^{II}}{\gamma C_{1111}^I + (1 - \gamma) C_{1111}^{II}}$$

$$C_{2211}^H = [\gamma C_{2211}^I (C_{1111}^I)^{-1} + (1 - \gamma) C_{2211}^{II} (C_{1111}^{II})^{-1}] \cdot \frac{C_{1111}^I C_{1111}^{II}}{\gamma C_{1111}^I + (1 - \gamma) C_{1111}^{II}}$$

$$C_{2222}^H = \frac{C_{2222}^I C_{2222}^{II}}{\gamma C_{2222}^I + (1 - \gamma) C_{2222}^{II}}, \quad C_{1212}^H = \frac{C_{1212}^I C_{1212}^{II}}{\gamma C_{1212}^I + (1 - \gamma) C_{1212}^{II}}$$

Table 2
Homogenized elastic tensor for rank-1 composite with isotropic phase materials

$$C_{1111}^H = \gamma E_I + (1 - \gamma) E_{II} + \frac{\nu^2}{1 - \nu^2} \frac{E_I E_{II}}{\gamma E_{II} + (1 - \gamma) E_I}, \quad C_{2211}^H = \frac{\nu}{1 - \nu^2} \frac{E_I E_{II}}{\gamma E_{II} + (1 - \gamma) E_I}$$

$$C_{2222}^H = \frac{\nu}{1 - \nu^2} \frac{E_I E_{II}}{\gamma E_{II} + (1 - \gamma) E_I}$$

$$C_{1212}^H = \frac{1}{2(1 + \nu)} \frac{E_I E_{II}}{\gamma E_{II} + (1 - \gamma) E_I}$$

Table 3
Homogenized elastic tensor for three-layer unit cell

$C_{1111}^H = \overline{A}(C_{1111}^I, C_{1111}^{II}, C_{1111}^{III}, \gamma_1, \gamma_2, \gamma_3) - \overline{A}((C_{2211}^I)^2(C_{1111}^I)^{-1}, (C_{2211}^{II})^2(C_{1111}^{II})^{-1}, (C_{2211}^{III})^2(C_{1111}^{III})^{-1}, \gamma_1, \gamma_2, \gamma_3) + \overline{A}^2(C_{2211}^I(C_{1111}^I)^{-1}, C_{2211}^{II}(C_{1111}^{II})^{-1}, C_{2211}^{III}(C_{1111}^{III})^{-1}, \gamma_1, \gamma_2, \gamma_3)\underline{A}(C_{1111}^I, C_{1111}^{II}, C_{1111}^{III}, \gamma_1, \gamma_2, \gamma_3)$
$C_{2211}^H = \overline{A}(C_{2211}^I(C_{1111}^I)^{-1}, C_{2211}^{II}(C_{1111}^{II})^{-1}, C_{2211}^{III}(C_{1111}^{III})^{-1}, \gamma_1, \gamma_2, \gamma_3) \cdot A(C_{1111}^I, C_{1111}^{II}, C_{1111}^{III}, \gamma_1, \gamma_2, \gamma_3)$
$C_{2222}^H = A(C_{2222}^I, C_{2222}^{II}, C_{2222}^{III}, \gamma_1, \gamma_2, \gamma_3), C_{1212}^H = \underline{A}(C_{1212}^I, C_{1212}^{II}, C_{1212}^{III}, \gamma_1, \gamma_2, \gamma_3)$

$$C_{1111}^i = C_{2222}^i = \frac{E_i}{1 - \nu^2}, \quad C_{2211}^i = \frac{\nu}{1 - \nu^2} E_i, \quad C_{1212}^i = \frac{E_i}{2(1 + \nu)} \quad (i = I, II, III) \tag{20}$$

The homogenized flexibility matrix is expressed as

$$S^H = (C^H)^{-1} = (C_{1111}^H C_{2222}^H C_{1212}^H - C_{1122}^H C_{2211}^H C_{1212}^H)^{-1} \begin{bmatrix} C_{2222}^H C_{1212}^H & & & \text{sym} \\ C_{2211}^H C_{1212}^H & C_{1111}^H C_{1212}^H & & \\ 0 & 0 & C_{1111}^H C_{2222}^H - C_{1122}^H C_{2211}^H & \\ & & & \end{bmatrix} \tag{21}$$

The equivalent Young’s modulus along the longitudinal direction is then

$$E_x^H = \frac{1}{S_{1111}^H} = C_{1111}^H - \frac{C_{1122}^H C_{2211}^H}{C_{2222}^H} \tag{22}$$

The corresponding beam deflection can be obtained as

$$w_{\max}^{\text{inf}} = \frac{FL^3}{3E_x^H I} = \frac{FL^3}{3(\gamma_1 E_I + \gamma_2 E_{II} + \gamma_3 E_{III}) \cdot \frac{b(2h)^3}{12}} = \frac{FL^3}{2(\gamma_1 E_I + \gamma_2 E_{II} + \gamma_3 E_{III}) \cdot bh^3} \tag{23}$$

In the current bending case, as the unit cell of the beam consists of three layers with thickness proportion of 1:1:1, i.e., $\gamma_1 = \gamma_2 = \gamma_3 = 1/3$ and $E_I = E_{III} = E_2, E_{II} = E_1$, Eq. (23) becomes

$$w_{\max}^{\text{inf}} = \frac{FL^3}{18b(E_1 + 2E_2)} \tag{24}$$

It is the same as the solution given in Eq. (9) for $n \rightarrow \infty$. This indicates that the homogenized solution is a limit value. The absolute error of the homogenized deflection solution relative to Eq. (9) is on the order of $O(\frac{1}{n^2})$ and reduces quadratically in terms of n .

2.3. Direct FE method

This is a direct numerical approach based on the finite element modeling of the entire structure. The discretization of each unit cell is refined with the increase of the cell size in order to keep the computing precision. Due to the periodicity, each cell can be regarded as a representative substructure for which the super-element condensation technique can be applied to reduce the computing time.

For the problem given in Fig. 2, each unit cell is discretized in the plane by four-node plane stress elements of the ANSYS software. The analytical deflections obtained from Eq. (6) are compared with the numerical ones and a good agreement between them is shown in Fig. 7 for different scale factors. Likewise, at $x = L/2$, variations of bending and shear stresses relative to n given in Figs. 8 and 9 show also a good agreement with analytical results given in Figs. 4 and 5, respectively. The relative error is less than 2%. The influence of scale factor n upon the maximum shear stress at $x = L/2$ is shown in Fig. 10. It is found that the maximum shear stress decreases as the scale factor n increases.

It is necessary to note that the relationship between the scale factor n and structural responses will change depending upon the material layout, i.e., material microstructure in the unit cell. For example, if all layers are aligned vertically along the thickness direction, the flexural rigidity will be kept unchanged even when n varies.

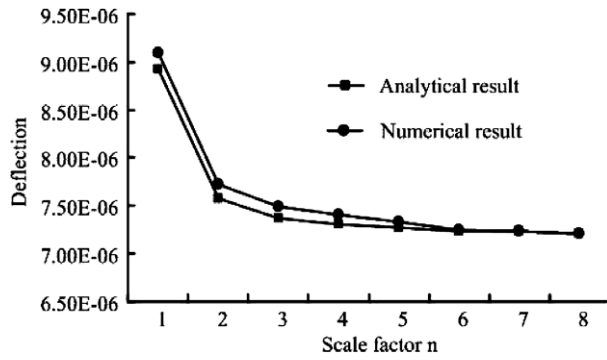


Fig. 7. Deflection variations versus the scale factor n at $x = L$.

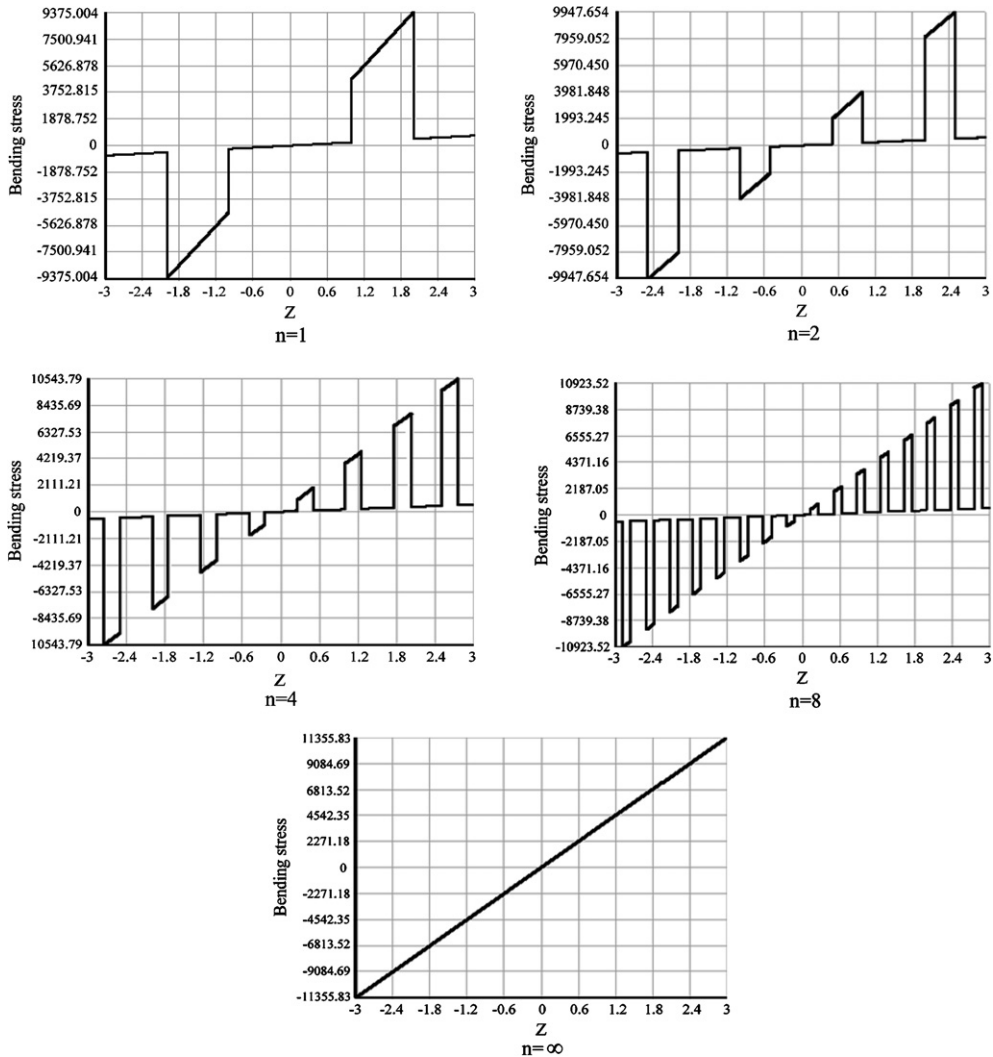


Fig. 8. FEM results of bending stress at $x = L/2$.

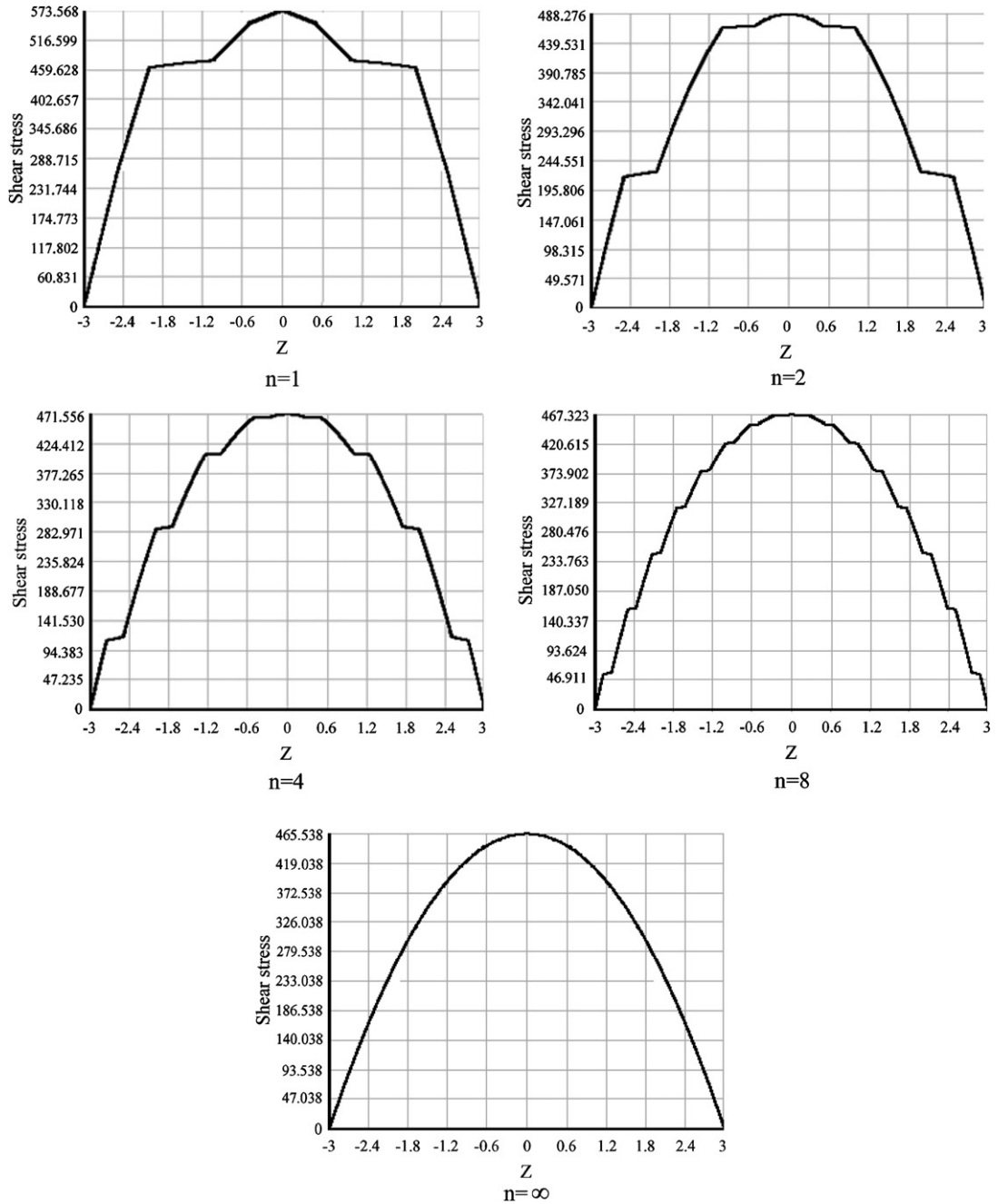


Fig. 9. FEM results of shear stress at $x = L/2$.

3. Examples

3.1. Multilayered circular tube in torsion

The similar study can be extended to torsion problems. For a circular tube of bi-phase materials illustrated in Fig. 11.

When $n = 1$, the torsion rigidity of the circular tube can be written as

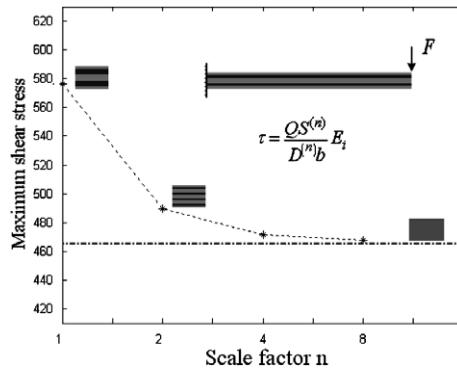


Fig. 10. Variations of maximum shear stress versus n at $x = L/2$.

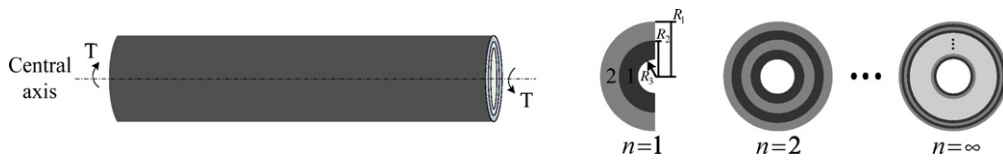


Fig. 11. Variations of cross-sectional configurations versus n .

$$J^{(1)} = G_2 \frac{\pi}{2} (R_1^4 - R_2^4) + G_1 \frac{\pi}{2} (R_2^4 - R_3^4) \tag{25}$$

Generally, the torsion rigidity can be written as

$$J^{(n)} = \sum G_i I_{pi} = G_2 \frac{\pi}{2} \sum_{m=1}^n \left\{ \left[\frac{mR_1 + (n-m)R_3}{n} \right]^4 - \left[\frac{(m-1)R_1 + R_2 + (n-m)R_3}{n} \right]^4 \right\} + G_1 \frac{\pi}{2} \sum_{m=1}^n \left\{ \left[\frac{(m-1)R_1 + R_2 + (n-m)R_3}{n} \right]^4 - \left[\frac{(m-1)R_1 + (n-m+1)R_3}{n} \right]^4 \right\} \tag{26}$$

where G_1 and G_2 represent the shear moduli of each material phase, respectively. Suppose three radiuses are $R_1 = 5$, $R_2 = 4$, $R_3 = 3$, the above relation reads

$$J^{(n)} = \sum G_i I_{pi} = G_2 \frac{\pi}{2} \sum_{m=1}^n \left[\left(\frac{5m + 3(n-m)}{n} \right)^4 - \left(\frac{5(m-1) + 4 + 3(n-m)}{n} \right)^4 \right] + G_1 \frac{\pi}{2} \sum_{m=1}^n \left[\left(\frac{5(m-1) + 4 + 3(n-m)}{n} \right)^4 - \left(\frac{5(m-1) + 3(n-m+1)}{n} \right)^4 \right] = \frac{\pi}{2} \left(272G_2 + \frac{98}{n}G_2 - \frac{1}{n^3}G_2 - \frac{98}{n}G_1 + \frac{G_1}{n^3} + 272G_1 \right) \tag{27}$$

The variation is described in Fig. 12 to show the scale effect. Note that due to the axisymmetry, the bending rigidity is just equal to a half of the torsional rigidity. When $n \rightarrow \infty$, the above relation becomes

$$J^{(inf)} = 136\pi(G_1 + G_2) \tag{28}$$

3.2. The LCA sandwich beam

The linear cellular alloys (LCA) belong to a sort of metal honeycombs that are manufactured by extrusion. Ordered holes of complex morphologies can be realized along the longitudinal direction to achieve desired

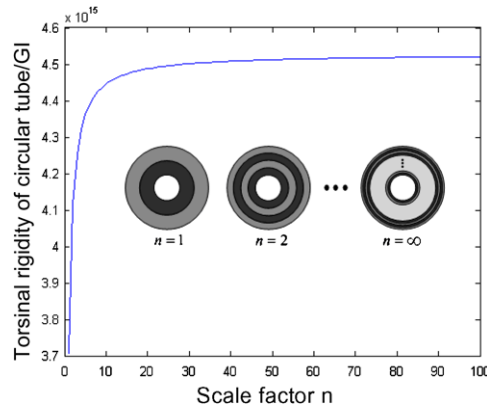


Fig. 12. Variations of the torsional rigidity versus n .

functionality. For this reason, it is interesting to study the hole size effect of the cellular beam upon its bending behaviors at the design stage. Here, square and circular holes are typically considered below. The proposed method can be used as a general one.

3.2.1. Rectangular cross-section with square holes

As shown in Fig. 13, the beam has an upper and bottom face sheets. The unit cell of the beam has two square holes in it when $n = 1$. In order to evaluate the effective flexural rigidity, the Boolean operation is used to subtract the contribution of holes. With this idea in mind, the general expression of the flexural rigidity for a cross-section with n unit cells can be expressed as

$$D^{(n)} = \sum E_i I_i = 2E_1 \frac{1}{3} b [(h_f + h_c)^3 - h_c^3] + 2E_2 \left\{ \frac{1}{3} b h_c^3 - \frac{1}{3} \frac{a}{n} \sum_{m=1}^n n \left[\left(\frac{(2m-1)h_c}{2n} + \frac{a}{2n} \right)^3 - \left(\frac{(2m-1)h_c}{2n} - \frac{a}{2n} \right)^3 \right] \right\} \tag{29}$$

Suppose $h_c = 2, h_f = 0.5, a = 1, b = 2$, we have then

$$D^{(n)} = 2 \left[5.0833E_1 + E_2 \left(5.3333 - \frac{4n^3 - 4n + 13}{3n^3} \right) \right] \tag{30}$$

In the case of $n \rightarrow \infty$, the limit value is

$$D^{(\text{inf})} = 2(5.0833E_1 + 4E_2) \tag{31}$$

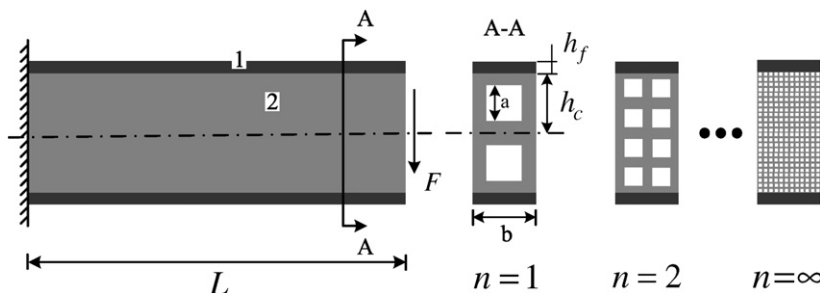


Fig. 13. LCA beam with ordered square holes.

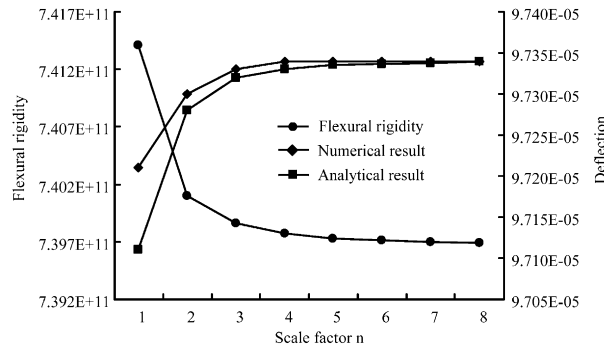


Fig. 14. Deflection and flexural rigidity variations versus the scale factor n at $x = L$.

The variation of flexural rigidity and the corresponding deflection compared with FE solution in Fig. 14 indicates a good agreement.

3.2.2. Rectangular section with circular holes

The configuration of the cross-section is shown in Fig. 15. The cross-section contains two identical holes for $n = 1$.

The flexural rigidity can be deduced in the same way.

$$D^{(n)} = \sum E_i I_i = 2E_1 \left[\frac{1}{3} b (h_f + h_c)^3 - h_c^3 \right] + 2E_2 \left\{ \frac{1}{3} b h_c^3 - n \sum_{m=1}^n \left[\frac{\pi}{2} \left(\frac{r}{n} \right)^4 + \left(\frac{2m-1}{2n} h_c \right)^2 \pi \left(\frac{r}{n} \right)^2 \right] \right\} \quad (32)$$

For $h_c = 2, h_f = 0.5, r = 1$ while other parameters are kept to be the same as before, the simplification leads to the compact form

$$D^{(n)} = 2 \left\{ 5.0833E_1 + E_2 \left[\frac{16}{3} - \left(\frac{\pi}{32n^2} + \frac{4n^3 - n}{12n^3} \pi \right) \right] \right\} \quad (33)$$

When $n \rightarrow \infty$, it becomes

$$D^{(inf)} = 2 \left[5.0833E_1 + E_2 \left(\frac{16}{3} - \frac{\pi}{3} \right) \right] \quad (34)$$

The variations of flexural rigidity and the corresponding deflection compared with FE solution are shown in Fig. 16.

3.2.3. Circular tube with triangular cell core (Wang and McDowell, 2003)

As illustrated in Fig. 17, such a beam bar was studied by Wang and McDowell (2003) and is reconsidered here.

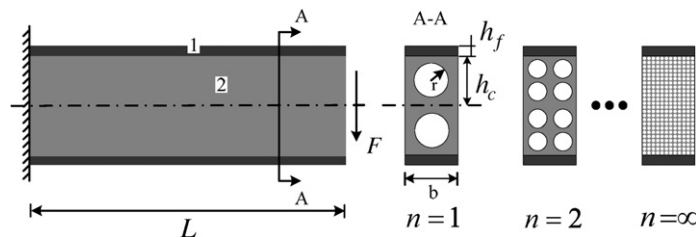


Fig. 15. LCA beam with ordered circular holes.

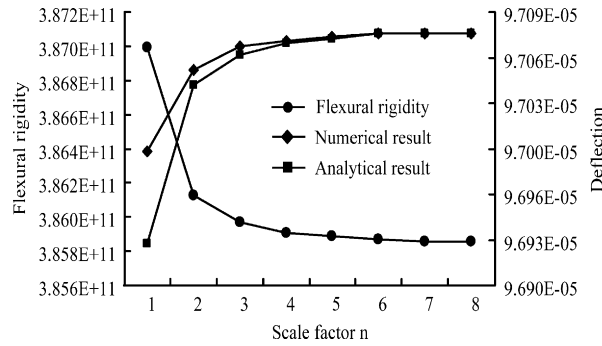


Fig. 16. Deflection and flexural rigidity variations versus n at $x = L$.

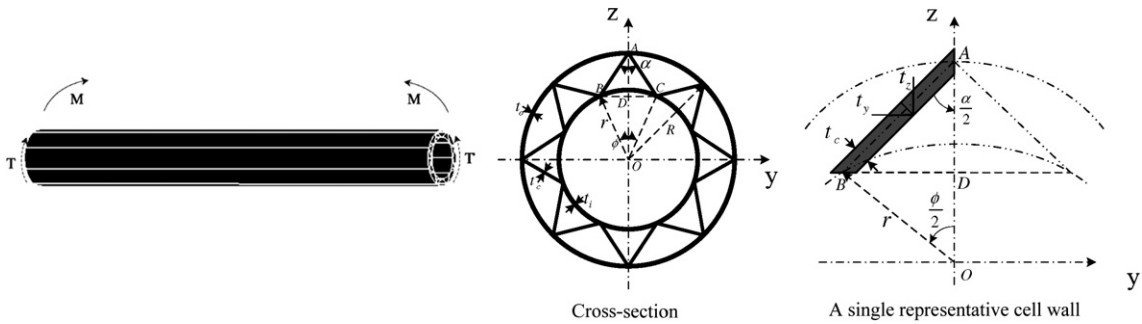


Fig. 17. Circular tube and its supercell with circle and triangle subcells.

Suppose the outside, inside face sheets and cell walls are made up of the same materials. Therefore, torsion and bending rigidity can be obtained as a summation of contributions from the core (c), inside sheet (i) and outside sheet (o).

$$J = J_c + J_i + J_o, \quad D = D_c + D_i + D_o \tag{35}$$

The angle of the unit cell defined from the center of the circle is designated as ϕ , whose relation with the whole number of unit cell, n , can be expressed as

$$n\phi = 2\pi \quad (n \geq 3) \tag{36}$$

In the paper of Wang and McDowell (2003), detailed studies are performed upon the rigidity design in terms of wall orientation. Here we are focused on the influence of n upon the rigidities while the cell wall thickness remains fixed. The general expressions of the torsional and bending rigidities are as follows and illustrated in Fig. 18.

$$J^{(n)} = G \left[2\pi(r^3 t_i + R^3 t_o) + \frac{2nt_c (Rr \sin \frac{\pi}{n})^2}{\sqrt{R^2 + r^2 - 2Rr \cos \frac{\pi}{n}}} \right] \tag{37}$$

$$\begin{aligned} D^{(n)} &= \frac{E}{2} [(I_y + I_z) + I_{po} + I_{pi}] = \frac{E}{2} \left[\left(\int_{z_B}^{z_A} z^2 t_y dz + \int_{y_B}^{y_A} y^2 t_z dy \right) + I_{po} + I_{pi} \right] \\ &= \frac{E}{6} t_y \left[R^3 - \left(R - r \cos \frac{\pi}{n} \right)^3 \right] + \frac{E}{6} t_z r^3 \sin^3 \frac{\pi}{n} + \frac{E}{2} (I_{po} + I_{pi}) \end{aligned} \tag{38}$$

with

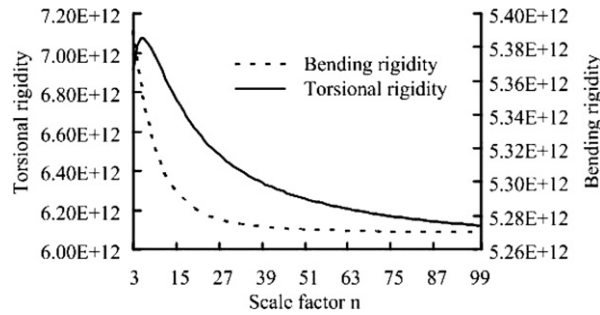


Fig. 18. Bending and torsional rigidity versus n .

$$I_{po} = \frac{\pi}{2} \left[\left(R + \frac{t_o}{2} \right)^4 - \left(R - \frac{t_o}{2} \right)^4 \right], \quad I_{pi} = \frac{\pi}{2} \left[\left(r + \frac{t_i}{2} \right)^4 - \left(r - \frac{t_i}{2} \right)^4 \right] \tag{39}$$

$$t_y = \frac{t_c}{\cos(\alpha/2)}, \quad t_z = \frac{t_c}{\sin(\alpha/2)}$$

and

$$\cos \frac{\alpha}{2} = \frac{\overline{AD}}{\overline{AB}} = \frac{R - \overline{OD}}{\overline{AB}} = \frac{R - r \cos \frac{\pi}{n}}{\sqrt{R^2 + r^2 - 2Rr \cos \frac{\pi}{n}}} \tag{40}$$

$$\sin \frac{\alpha}{2} = \frac{\overline{BD}}{\overline{AB}} = \frac{r \sin \frac{\pi}{n}}{\sqrt{R^2 + r^2 - 2Rr \cos \frac{\pi}{n}}}$$

3.3. Sandwich beam with periodically variable cross-section

Here, we will study another sort of sandwich beams that have periodically variable cross-sections along the longitudinal direction.

3.3.1. Sandwich beam with square holes

A sandwich beam with square holes is shown in Fig. 19. Suppose the upper and lower face sheets have a common thickness of h_f . Note a is defined as the hole size related to $n = 1$. Under the assumption of fixed volume fraction of the solid material phase, the configuration variation of the beam in terms of the size factor n is illustrated. To reveal the relationship between the equivalent beam bending stiffness, $D^{(n)}$, and n , the energy-equivalence method is employed here. Namely, the strain energy of the beam, $U_b^{(n)}$, associated with equivalent stiffness, $D^{(n)}$, is equal to the summed contribution of all struts in the original beam. Hence, due to the cell periodicity along the beam length, the strain energy can be calculated over one periodic length l . Under the pure bending load, the strain energy can be written as

$$U_b^{(n)} = \frac{1}{2} \frac{M^2 l}{D^{(n)}} = \frac{M^2}{2} \int_0^l \frac{1}{D(x)} dx \tag{41}$$

in which the integral can be evaluated as a summation over the periodical length so that

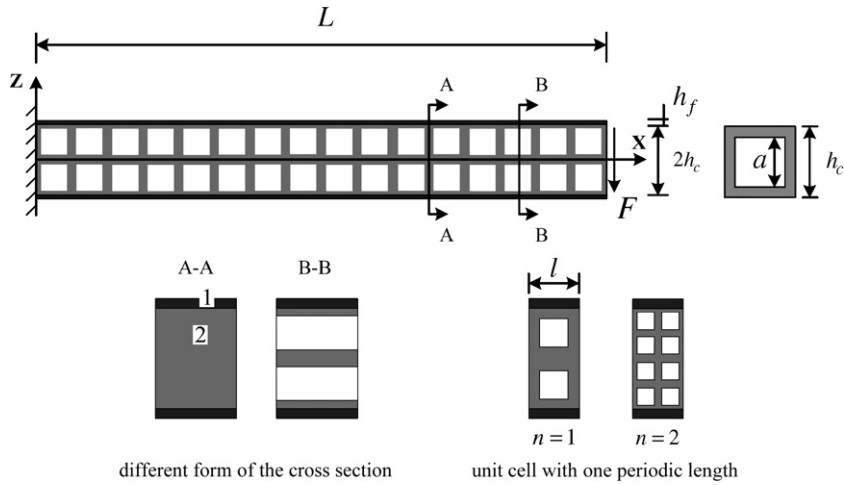


Fig. 19. Sandwich beam with periodically variable cross-section.

$$D^{(n)} = \left(\frac{1}{l} \int_0^l \frac{1}{D(x)} dx \right)^{-1} = l \left(\sum_i \frac{l_i}{D_i} \right)^{-1} \quad (42)$$

$$D^{(n)} = \frac{2}{3} E_1 b [(h_c + h_f)^3 - h_c^3] + \frac{E_2 l_1 l_2}{\frac{h_c - a}{h_c} l_2 + \frac{a}{h_c} l_1} \quad (43)$$

$$I_1 = \frac{2}{3} b h_c^3, \quad I_2 = \frac{2}{3} b h_c^3 - \frac{2}{3} b \sum_{m=1}^n \left[\left(\frac{(2m-1)h_c + a}{2n} \right)^3 - \left(\frac{(2m-1)h_c - a}{2n} \right)^3 \right] \quad (43)$$

$$D^{(\text{inf})} = \frac{2}{3} E_1 b [(h_c + h_f)^3 - h_c^3] + \frac{2}{3} \frac{E_2 b h_c^4 (b h_c - a)}{b h_c^3 - a h_c + a^2} \quad (44)$$

For example, consider the following case: core material properties of $E_2 = 3.5E_9$, $\nu_2 = 0.34$, face sheet material properties of $E_1 = 70E_9$, $\nu_1 = 0.34$ and beam dimensions of $L = 60$, $h_f = 0.1$, $h_c = 1.5$, $a = 1$, the volume fraction is $\alpha = 1 - (a^2/h_c^2) = 0.56$. Correspondingly, flexural rigidity and deflection are evaluated and shown in Fig. 20.

To validate the computing, analytical solutions are compared with FE results. Assume the beam is discretized by a refined mesh of 100×10 four-node plane stress elements. By increasing the value of n successively, tip deflections obtained are compared in Fig. 21. Note that when $n \rightarrow \infty$, the FE solution is achieved based on the homogenized bending rigidities.

It is shown that both numerical and analytical deflection results are consistent. They become bigger and tend to the limit value evaluated by the homogenization method as n increases.

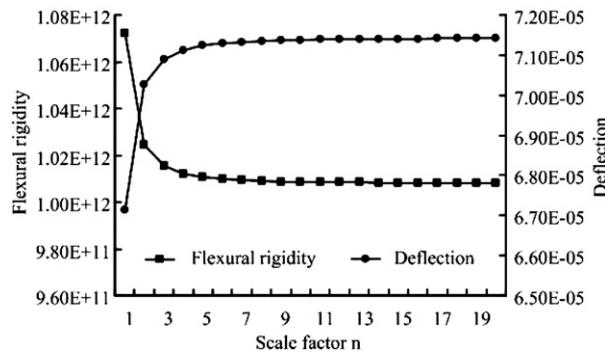


Fig. 20. Flexural rigidity and tip deflection of the square-hole sandwich beam versus n .

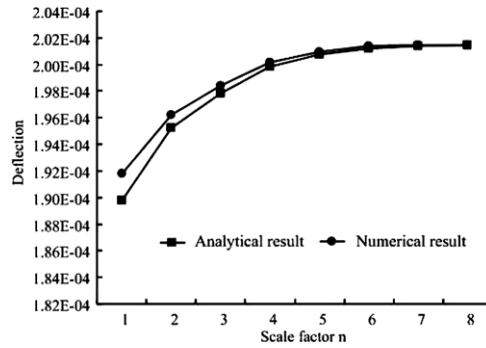


Fig. 21. Deflection variations versus the scale factor n at $x = L$.

Moreover, it is interesting to study the accuracy of the proposed energy-equivalence method for different values of volume fraction, α , and the effect of the latter upon the tip deflection. To do this, we change progressively the hole size, a , while h_c remains constant. Numerical and theoretical results of tip deflection are compared in Fig. 22 when the volume fraction α varies from 0.1 to 0.9. It is observed that generally, the energy-equivalence method has a good agreement with the FE method. $\alpha = 0.3$ is roughly a critical value below which the deviation of tip deflection results obtained by both methods is relatively important but the maximum relative error is under 6%.

3.3.2. Sandwich beam with other holes

According to the energy-based method given in Eq. (42), the effective flexural rigidities can be thus derived in the same way for sandwich beams of other cell types in terms of the scale factor n . Here, typical configurations of circle, cross and hexagon cells are taken into account. Detailed developments are omitted and expressions of closed form are given in Table 4. It should be noticed that the contribution of face sheets is not included in each expression and that dimensions associated with the cell configurations in the left column of Table 4 correspond to the sizes of $n = 1$. Besides, to have an idea about the structural efficiency of different cell configurations, the same volume fraction $\alpha = 0.56$, i.e., the same structural weight is used in the following computing to make easy the comparison.

- For the sandwich beam with circle holes, if initial data are $L = 60$, $h_f = 0.1$, $h_c = 1.5$, $r = 0.5614$, both theoretical and FEM results of tip deflection are illustrated in Fig. 23.
- For the sandwich beam with cross-holes, assume the initial data are $L = 60$, $h_f = 0.1$, $h_c = 1.5$, $r = 0.7071$. Both theoretical and FEM results are illustrated in Fig. 24.
- For the sandwich beam with cross-holes, assume the initial data are $L = 1$, $h_f = 0.1$, $h_c = 2$, $a = 0.7887$, $e = 0.6431$, both theoretical and FEM results are illustrated in Fig. 25.

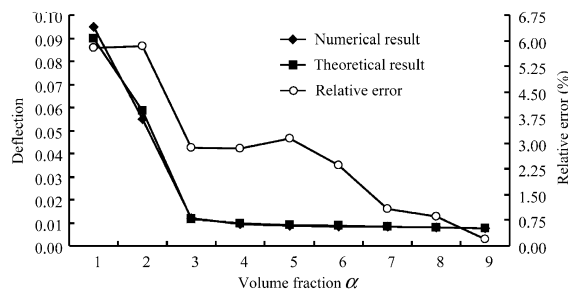
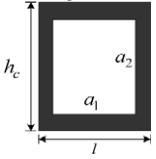
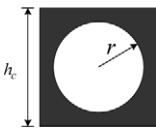
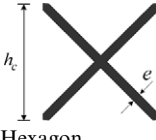
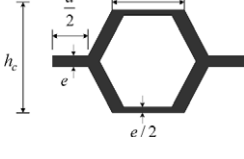


Fig. 22. The comparison of numerical and theoretical results for different values of volume fraction.

Table 4
Equivalent bending stiffness and their limit values ($n \rightarrow \infty$) for different cell forms

Cell type	Equivalent bending stiffness (EBS)	Limit of EBS ($n \rightarrow \infty$)
	$D^{(n)} = \frac{EI_1 I_2}{l - a_1 I_2 + a_1 I_1}$ $I_1 = \frac{1}{3} b h_c^3$ $I_2 = \frac{1}{3} b h_c^3 - \frac{1}{3} b \sum_{m=1}^n \left[\left(\frac{(2m-1)h_c + a_2}{2n} \right)^3 - \left(\frac{(2m-1)h_c - a_2}{2n} \right)^3 \right]$ $= \frac{1}{3} b h_c^3 - \frac{1}{12n^3} [4h_c^2 a_2 (n^3 + 2) + n a_2^3]$	$D^{(\text{inf})} = \frac{1}{3} \frac{E b h_c^4 (b h_c - a_2)}{b h_c^2 - h a_2 + a_1 a_2}$
	$D^{(n)} = \frac{1}{h_c} \left\{ \int_0^{\frac{h_c-r}{2n}} \frac{1}{E_2 (\frac{1}{3} b h_c^3)} dx + \int_{\frac{h_c-r}{2n}}^{\frac{h_c+r}{2n}} \frac{1}{E_2 \left\{ \frac{1}{3} b h_c^3 - \frac{1}{3} n b \sum_{m=1}^n \left[\left(\frac{(2m-1)h_c}{2n} + \sqrt{\left(\frac{r}{n} \right)^2 - \left(x - \frac{(2m-1)h_c}{2n} \right)^2} \right)^3 - \left(\frac{(2m-1)h_c}{2n} - \sqrt{\left(\frac{r}{n} \right)^2 - \left(x - \frac{(2m-1)h_c}{2n} \right)^2} \right)^3 \right] \right\}} dx + \int_{\frac{h_c+r}{2n}}^{\frac{h_c}{n}} \frac{1}{E_2 (\frac{1}{3} b h_c^3)} dx \right\}^{-1}$	–
	$D^{(n)} = \frac{h_c}{n} \frac{\frac{4\sqrt{3}E(\frac{\sqrt{2}e}{2n})^2}{3}}{\sum_{m=1}^n \left[\arctan \left(\frac{\frac{m}{\sqrt{3}} h_c}{\frac{\sqrt{3}\sqrt{2}e}{3-2n}} \right) - \arctan \left(\frac{\frac{m-1}{\sqrt{3}} h_c}{\frac{\sqrt{3}\sqrt{2}e}{3-2n}} \right) \right]}$ $= \frac{h}{n} \frac{\frac{4\sqrt{3}E(\frac{\sqrt{2}e}{2n})^2}{3}}{\arctan \left(\frac{n\sqrt{6}h_c}{3-2n} \right) - \arctan \left(\frac{\sqrt{6}h_c}{e} \right)}$	$D^{(\text{inf})} = 0$
	$\frac{1}{D^{(n)}} = \frac{1}{2E} \sum_{m=1}^n \left[\frac{1}{\left(\frac{2m-1}{2n} h_c + \frac{e}{2n} \right)^3} - \frac{1}{\left(\frac{2m-1}{2n} h_c - \frac{e}{2n} \right)^3} \right]$ $+ \frac{2n^3}{4\sqrt{3}Eae^2} \sum_{m=1}^n \left[\arctan \frac{m}{\sqrt{3}} - \arctan \frac{m-1}{\sqrt{3}} \right]$ $+ \frac{1}{2E} \sum_{m=1}^n \left\{ \left[\frac{1}{\left(\frac{2m-1}{2n} h_c \right)^3} - \frac{1}{\left(\frac{2m-1}{2n} h_c - \frac{e}{2n} \right)^3} \right] + \left[\frac{1}{\left(\frac{m-1}{n} h_c + \frac{e}{2n} \right)^3} - \frac{1}{\left(\frac{m-1}{n} h_c \right)^3} \right] \right\}$ $= \frac{16n^2}{E[h_c^2 a(4n^2 - 1) + a^2]} + \frac{\sqrt{3}n^3}{2Eae^2} \left(\arctan \frac{3na}{e} - \arctan \frac{3a}{e} \right)$ $+ \frac{4n^2}{2e^3 + 6n^2 e^2 h_c + e h_c^2 (8n^2 + 6n + 1) + 3eh_c(n-1)}$	$D^{(\text{inf})} = 0$

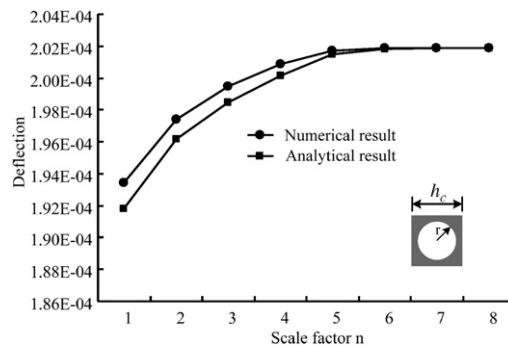


Fig. 23. Deflection variations versus the scale factor n for sandwich beam with circle holes.

Finally, tip deflections of a sandwich beam using four different types of cell configurations with the same face sheet are compared in Fig. 26. If the structural efficiency is concerned with the maximum rigidity, the square-hole beam is shown to have the smallest deflection for the same volume fractions of core material.

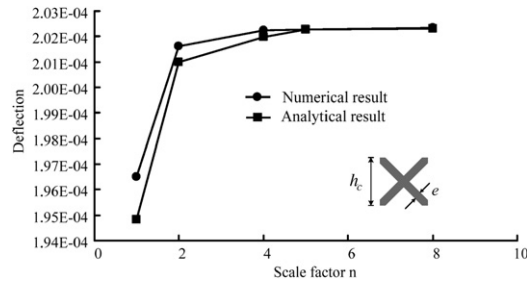


Fig. 24. Deflection variations versus the scale factor n for sandwich beam with cross-hole.

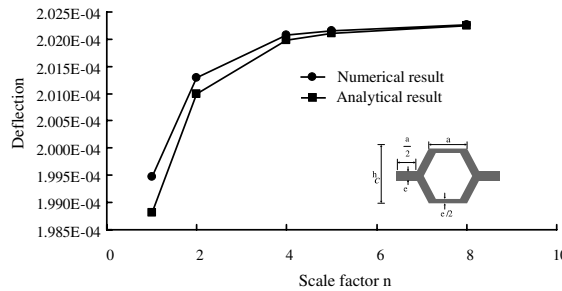


Fig. 25. Deflection variations versus the scale factor n at $x = L$ for cross-hole sandwich beam.

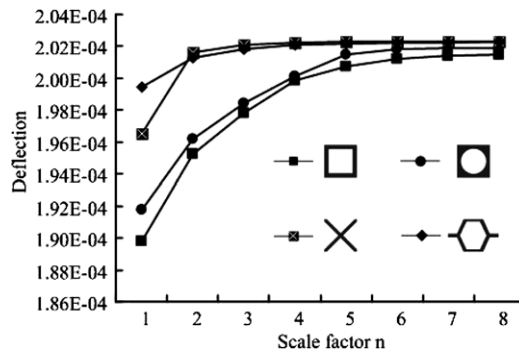


Fig. 26. Deflections of sandwich beams with different cell forms versus n ($\alpha = 0.56$).

4. Conclusions

In this paper, scale effect of the basic cell is highlighted in the static analysis of sandwich beams. Abundant examples are taken into account. Typical cell configurations are studied by classic beam theory, homogenization method and FE method in a systematic way. Relations of closed form are established between the static responses and scale factor n based on the classic beam theory. Flexural, torsion and stretch rigidities are distinguished to show their dependences upon the scale factor. The validity of the homogenization method is clarified in comparison to the analytical method although the former is commonly used in the numerical prediction and design of composite materials. It is demonstrated that the homogenized solution is the limit value whenever the scale factor tends to be infinitely large. However, the homogenization is found to be of high precision when the scale factor n takes the value large enough. This is because the influence of scale factor is on the order of $O(1/n^2)$. Finally, it is necessary to notice that although the developed work is limited to the static analysis, the proposed procedures can be generalized to deal with thermal mechanical, dynamic, buck-

ling and other kinds of problems. The scale factor is an important parameter to evaluate the structural efficiency when the cell size is designed.

Acknowledgments

Thanks for the helpful comments of anonymous reviewers to improve the quality of the paper. This study is supported by the 973 Program (Grant No. 2006CB601205), Natural Science Foundation of China (Grant No. 90405016, 10676028), 863 Program (Grant No. 2006AA04Z122), Doctoral Research Foundation (Grant No. 20060699006) and Doctorate Foundation of Northwestern Polytechnical University (CX200610).

References

- Abrate, S., 2006. Free vibration, buckling, and static deflections of functionally graded plates. *Composites Science and Technology* 66, 2383–2394.
- Ashby, M.F., 1999. *Materials Selection in Mechanical Design*, second ed. Butterworth Heinemann, Oxford.
- Ashby, M.F., Bréchet, Y.J.M., 2003. Designing hybrid materials. *Acta Materialia* 51, 5801–5821.
- Bakhvalov, N.S., Panasenko, G.P., 1989. *Averaging Processes in Periodic Media. Mathematical Problems in Mechanics of Composite Materials*. Kluwer, Dordrecht.
- Bendsøe, M.P., Sigmund, O., 2003. In: *Topology Optimization: Theory, Methods and Applications*. Springer, Berlin.
- Bendsøe, M.P., Triantafyllidis, N., 1990. Scale effects in the optimal design of a microstructured medium against buckling. *International Journal of Solids and Structures* 26 (7), 725–741.
- Bensoussan, A., Lions, J.-L., Papanicolaou, G., 1978. *Asymptotic Methods for Periodic Structures*. North-Holland, Amsterdam.
- Burgueno, R., Quagliata, M.J., Mohanty, A.K., Mehta, G., Drzal, L.T., Misra, M., 2005. Hierarchical cellular designs for load-bearing biocomposite beams and plates. *Materials Science and Engineering A* 390 (1–2), 178–187.
- Burton, W.S., Noor, A.K., 1997. Assessment of continuum models for sandwich panel honeycomb cores. *Computer Methods in Applied Mechanics and Engineering* 145, 341–360.
- Fujii, D., Chen, B.C., Kikuchi, N., 2001. Composite material design of two-dimensional structures using the homogenisation method. *International Journal for Numerical Methods in Engineering* 50, 2031–2051.
- Hassani, B., Hinton, E., 1998. A review of homogenization and topology optimization II-analytical and numerical solution of homogenization equations. *Computers and Structures* 69, 719–738.
- Hayes, A.M., Wang, A.-j., Dempsey, B.M., McDowell, D.L., 2004. Mechanics of linear cellular alloys. *Mechanics of Materials* 36, 691–713.
- Hsueh, C.H., Luttrell, C.R., Becher, P.F., 2006. Modelling of bonded multilayered disks subjected to biaxial flexure tests. *International Journal of Solids and Structures* 43, 6014–6025.
- Khdeir, A.A., Reddy, J.N., 1997. An exact solution for the bending of thin and thick cross-ply laminated beams. *Composite Structures* 37, 195–203.
- Kolpakov, A.G., 2001. Solution of the problem of design of laminated plates possessing the given stiffness. *International Journal of Solids and Structures* 38, 6015–6025.
- Meraghni, F., Desrumaux, F., Benzeggagh, M.L., 1999. Mechanical behaviour of cellular core for structural sandwich panels. *Composites Part A* 30, 767–779.
- Neves, M.M., Sigmund, O., Bendsøe, M.P., 2002. Topology optimization of periodic microstructures with a penalization of highly localized buckling modes. *International Journal for Numerical Methods in Engineering* 54, 809–834.
- Noor, A.K., Burton, W.S., Bert, C.W., 1996. Computational models for sandwich panels and shells. *Applied Mechanics Reviews* 49 (3), 155–199.
- Onck, P.R., Andrews, E.W., Gibson, L.J., 2001. Size effects in ductile cellular solids. Part I: modeling. *International Journal of Mechanical Sciences* 43, 681–699.
- Pasini, D., 2006. Shape transformers for material and shape selection of lightweight beams. *Materials and Design*. doi:10.1016/j.matdes.2006.05.028.
- Romanoff, J., Varsta, P., 2006. Bending response of web-core sandwich beams. *Composite structures* 73, 478–487.
- Sanchez-Palencia, E., 1980. Non-homogeneous media and vibration theory. In: *Lecture Notes in Physics*, vol. 127. Springer, Berlin.
- Tantikom, K., Aizawa, T., Mukai, T., 2005. Symmetric and asymmetric deformation transition in the regularly cell-structured materials Part I: experimental study. *International Journal of Solids and Structures* 42, 2199–2210.
- Wang, A.J., McDowell, D.L., 2003. Optimization of a metal honeycomb sandwich beam-bar subjected to torsion and bending. *International Journal of Solids and Structures* 40, 2085–2099.
- Zhang, W.H., Sun, S.P., 2006. Scale-related topology optimization of cellular materials and structures. *International Journal for Numerical Methods in Engineering* 68, 993–1011.